Photoactivated Nanoscale Temperature Gradient Detection Using X-ray Absorption Spectroscopy as a Direct Nanothermometry Method

Ana Espinosa, German Castro, Javier Reguera, Carlo Castellano, Javier Castillo, Julio Camarero, Claire Wilhelm, Miguel Angel García, Álvaro Muñoz-Noval

Supplementary Information

Photoactivated Nanoscale Temperature Gradient Detection Using X-ray Absorption Spectroscopy as a Direct Nanothermometry Method

Ana Espinosa[1,2], German R. Castro[3,4], Javier Reguera[5], Carlo Castellano[6], Javier Castillo[1], Julio Camarero[1,7], Claire Wilhelm[8], Miguel Angel García[9], Álvaro Muñoz-Noval[10*]*

[1] IMDEA Nanociencia, c/ Faraday, 9, 28049 Madrid, Spain

[2]Nanobiotecnología (IMDEA-Nanociencia), Unidad Asociada al Centro Nacional de Biotecnología (CSIC), 28049 Madrid, Spain

[3] Spanish CRG beamline at the European Synchrotron (ESRF), B.P. 220, F-38043 Grenoble, France

[4]Instituto de Ciencia de Materiales de Madrid, ICMM-CSIC, 28049 Madrid, Spain

[5] BCMaterials, Basque Center Centre for Materials, Applications and Nanostructures, UPV/EHU Science Park, 48940 Leioa, Spain

[6] Dipartimento di Chimica, Università degli Studi di Milano, via Golgi 19, 20133 Milano, Italy

[7] Departamento de Física de la Materia Condensada and Instituto 'Nicolás Cabrera', Universidad Autónoma de Madrid, 28049 Madrid, Spain

[8] Laboratoire Matière et Systèmes, Complexes MSC, UMR 7057, CNRS & University Paris Diderot, 75205, Paris Cedex 13, France

[9] Departamento de Electrocerámica, Instituto de Cerámica y Vidrio, ICV-CSIC, Kelsen 5, 28049 Madrid, Spain

[10] Dpto. Física Materiales, Facultad CC. Físicas, Universidad Complutense de Madrid, 28040 Madrid, Spain

E-mail: address correspondence to ana.espinosa@imdea.org, almuno06@ucm.es.

Contents:

I. Thermal conductive and radiative mechanisms of heat nanogenerators

The radiative heat transfer (q_R) depends on the emissivity (ε) of the NP, the contact surface (A_{NP}) and the difference of the fourth-power of the temperature of the NP and the matrix as:

$$q_R = \varepsilon k_B A_{NP}(T_{NP}^4 - T_{matrix}^4) \quad \text{Eq. 1}$$

being k_B the Boltzman constant (1.38×10^{-23} J. K^{-1}). We can estimate the order of this heat transfer by setting up specific values, such as 20 nm for the NP radius, a consistent value of 0.06 for gold emissivity and 100 ºC in the NP and room temperature for the matrix. With these values, a radiative heat transfer in the 10^{-14} W range is obtained.

Concerning the second mechanism (conduction), the conductive heat transfer in the surrounding of a nano-object cannot be understood in the framework of Fourier heat transport[1] because non-local and non-equilibrium effects take place in the local surrounding of the NP. This results in a less efficient heat transport and in a lower heat transfer rate. However, Chen et al.[2] developed a simple expression to quantify the heat transfer in a nano-object. If we consider the same nanoparticle as in Fig. 1A, the effective ballistic conductive heat transfer can be expressed as:

$$q_C = k\frac{\tau_{NP}}{r_{NP}(4/3+\tau_{NP})}A_{NP}(T_{NP} - T_{matrix}) \quad \text{Eq. 2}$$

where k is the thermal conductivity and $\tau_{NP} = r_{NP}/\lambda_l$ a dimensionless parameter that ponderates the NP radius to the mean free path of the heat carriers (λ_l), that in case of metallic nanoparticles, these are electrons. Using the values for gold, this expression gives heat transfer

in the 10^{-4} W range, much larger than the radiative, but, according to Chen et al.[2], this mechanism results in heat conductivity lower than two orders of magnitude (for Au NPs of about 20 nm) than it is found in the diffusive limit. The heat transfer between the hot NP and the matrix is threfore less efficient due to the ballistic heat transport, it becomes then more difficult to dissipate heat through the surface of the NPs, which leads to an increase of increasing orders of magnitude the thermal gradient around the NP.

II. Experimental methods

Nanoparticle fabrication

Gold nanorods

Rod shape gold nanomaterials with an approximate aspect ratio of 3.5 (length 41 nm, diameter 11 nm) were synthesized following a seed-mediated growth method previously described[3-4]. Initially, gold seed particles were obtained by adding $HAuCl_4$ (1 mL, 5×10^{-4} M) to a solution of CTAB (1 mL, 0.2 M) and with an ice-cold $NaBH_4$ (0.12 mL, 0.01 M). The mixture was vigorously stirred for several minutes minutes at 1800 rpm on an orbital shaker. Then, $HAuCl_4$ (50 mL, 0.01 M), $AgNO_3$ (4×10^{-3} M, 50 mL), CTAB (50 mL, 0.2 M) and ascorbic acid (0.7 mL, 0.078 M) were sequentially added to 0.12 mL of the previous prepared gold seeds solution. The mixture reacted for 30 minutes at 1200 rpm of stirring Finally, the formed gold nanorods were separated by centrifugation (14000 rpm, 10 minutes) and resuspended in water.

Gold-iron oxide nanostars

The gold-iron oxide magnetic nanostars were synthesized as previously reported.[5] Its synthesis is based on a seed-mediated growth process starting with preformed heterodimer seeds of gold:iron oxide with diameters of 6 and 20 nm respectively. A nanostar growing step is performed in a dimethylformamide solution of chloroauric acid and polyvinylpyrrolidone. The reaction takes place at room temperature, and the nanoparticles are purified by several centrifugation steps and finally resuspended in water.

UV-vis-NIR spectroscopy

UV-vis-NIR spectra were obtained using a Cary Spectrometer (Varian) in the 300–1100 nm spectral range.

Transmission Electron Microscopy

TEM examination of nanomaterials was done using a JEOL JEM-1400PLUS instrument operating at 120 kV. The nanomaterials were deposited on carbon-coated TEM grids. The nanoparticles morphological features were analyzed with the ImageJ software package.

X-ray absorption measurements (XAS)

XAS measurements were performed at the CRG beamline (BM25-SpLine) of the European Synchrotron Radiation Facilities (ESRF) in Grenoble (France). Powder samples cointaing a fraction of Au-based nanomaterials (AuNR or AuNS) in a boron nitride (BN) matrix were homogenized and pressed into pellets hat were then held in a sample holder between two layers of kapton tape. The spectra were acquired at the Au L-edge (11 919 eV) comprising the two energy regimes: XANES (X-ray absorption near edge structure) and in the EXAFS (extended X-ray absorption fine structure). The measurements were obtained at different temperatures (from 10 K to 350 K) using a liquid helium-nitrogen cryostat with vacuum/He-gas insulation/contact gas. The spectra were collected in the transmission mode using ionization chambers as detectors. This mode is preferred since they provide a higher signal to-noise ratio than in fluorescence mode. A Au foil was measured as a reference and during the measurements to correct energy drifts by using a third ionization chamber. At each laser condition, 4 to 5 XAS spectra were acquired and averaged to discard beam and thermal fluctuations. A total time of 2 h was employed per sample and experimental condition. Data normalization and background subtraction of the XAS data were carried out using the Athena program[6]. The spectra were subjected to a background subtraction.

Temperature-dependent EXAFS measurements

Artermis program was used to extract and process the normalized EXAFS signal as a function of the photoelectron wavevector, k, χ(k) in the range of 2 and 10 $Å^{-1}$ [6]. The data were examined in the R-space by Fourier transforming the χ(k) signal. A window function is used to minimize Fourier transform artefacts. Structural information of Au-based nanomaterials was extracted by fitting the experimental EXAFS spectra (for each temperature condition). The structural parameters obtained at each fitting and temperature were the coordination number (N), the average Au–Au bond length (R), and the EXAFS Debye–Waller factor (σ^2) using the FEFF code[7].

NIR laser-induced heating measurements

Photothermal excitation on Au-based nanomaterials was carried out using a NIR 808-nm laser coupled of 1 W maximum power (Roithner Lasertechnik GmbH). The samples were illuminated wih a regulated power using an optical atenuator placed in between the laser and the sample. The laser light was irradiated the sample at the same time as X-rays beam in the experimental hood of the CRG BM25 beamline. The distance between the sample and the laser was set so as the laser spot was 0.25 cm^2, larger than that of the X-ray beam area illumination.

Macroscopic temperature determination

The temperature elevation curves under laser excitation were recorded using an infrared thermal (IR) imaging camera (FLIR T540, USA). The IR camera was placed in two different positions considering the configuration geometry of laser and X-rays illumination.

III. Supplementary figures and tables

Supplementary figures

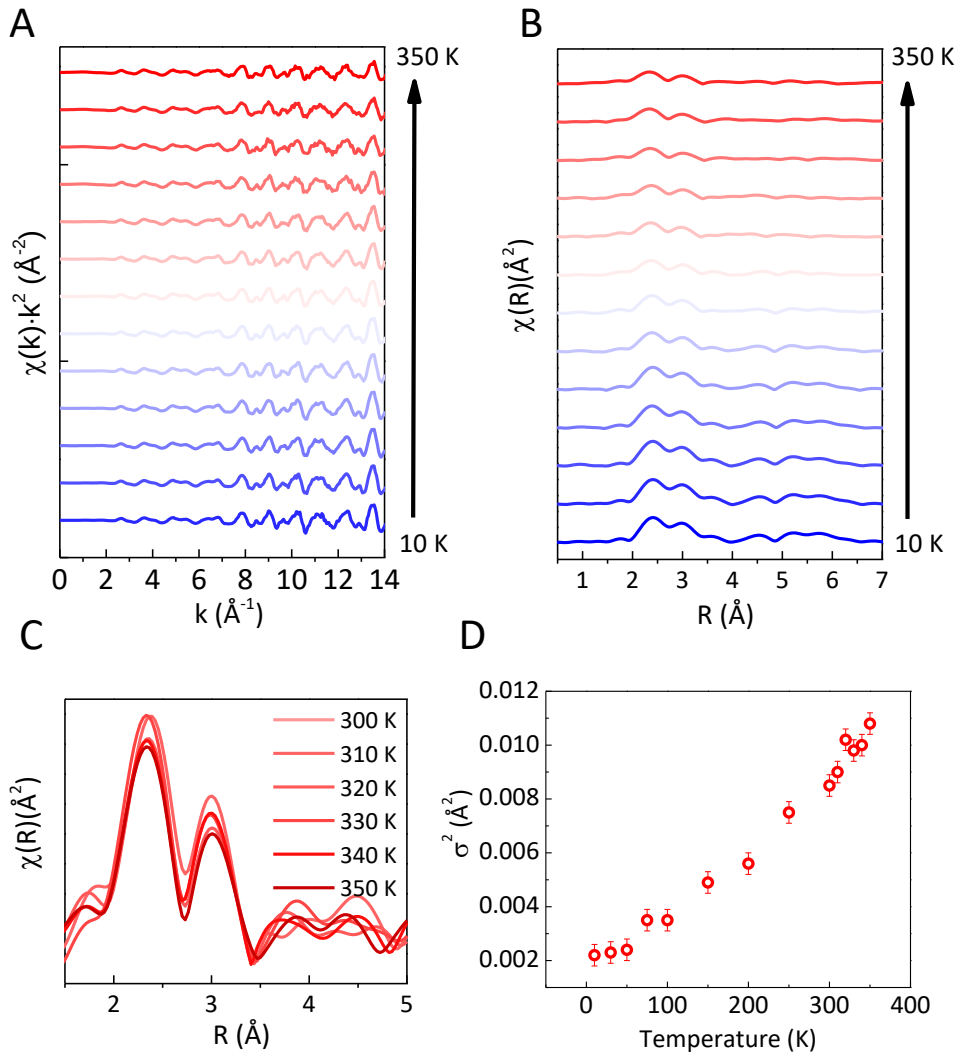

Figure S1. **Thermal calibration of structural parameters of AuNS from temperature dependent EXAFS measurements**. (A) EXAFS spectra and (B) FT of the EXAFS signal from 10 to 350 K. (C) FT of the EXAFS signal in the range of calibration from 300 to 350 K. (D) Debye–Waller factor (σ^2) of AuNS as a function of temperature obtained through the fits to the experimental EXAFS data, both independent of the Einstein model.

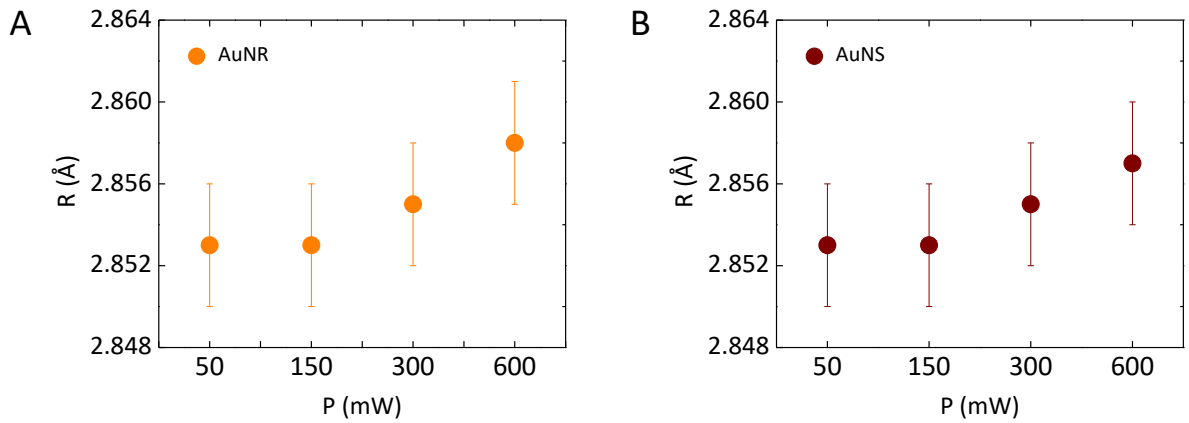

Figure S2. Average Au–Au bond length (R) of single and hybrid gold-based nanomaterials under laser irradiation. Average Au–Au bond length (R) for AuNR and AuNS subjected to different laser powers.

Supplementary tables

Laser power (mW)	Nanorods AuNR					Nanostars AuNS				
	N	R (Å)	σ^2(Å^2)	T (K)	ΔT (ºC)	N	R (Å)	σ^2(Å^2)	T(K)	ΔT (ºC)
50	9.6	2.853(3)	0.0087(4)	314(5)	19(5)	10.8	2.853(3)	0.0086(4)	325(5)	31(5)
150	9.6	2.853(3)	0.0091(4)	332(5)	37(5)	10.8	2.853(3)	0.0089(4)	336(5)	42(5)
300	9.6	2.855(3)	0.0097(3)	357(4)	62(4)	10.8	2.855(3)	0.0095(4)	356(5)	62(5)
600	9.6	2.858(3)	0.0111(3)	418(4)	123(4)	10.8	2.857(3)	0.0107(4)	400(5)	106(5)

Table S1. *In situ* temperature values obtained by fitting the experimental structural parameters (coordination number (N), the average Au–Au bond length (*R*), and the EXAFS Debye–Waller factor (σ^2) from EXAFS data of AuNR and AuNS under NIR-laser excitation.

IV. References

1. Chen, G., Nonlocal and nonequilibrium heat conduction in the vicinity of nanoparticles. *Journal of Heat Transfer* **1996,** *118*, 539-545.

2. Chen, G., Ballistic-diffusive heat-conduction equations. *Physical Review Letters* **2001,** *86* (11), 2297.

3. Orendorff, C. J.; Murphy, C. J., Quantitation of metal content in the silver-assisted growth of gold nanorods. *J. Phys. Chem. B* **2006,** *110* (9), 3990-3994.

4. Espinosa, A.; Kolosnjaj-Tabi, J.; Abou-Hassan, A.; Plan Sangnier, A.; Curcio, A.; Silva, A. K.; Di Corato, R.; Neveu, S.; Pellegrino, T.; Liz-Marzán, L. M., Magnetic (Hyper) Thermia or Photothermia? Progressive Comparison of Iron Oxide and Gold Nanoparticles Heating in Water, in Cells, and In Vivo. *Adv. Funct. Mater.* **2018,** *28* (37), 1803660.

5. Reguera, J.; Jiménez De Aberasturi, D.; Henriksen-Lacey, M.; Langer, J.; Espinosa, A.; Szczupak, B.; Wilhelm, C.; Liz-Marzán, L. M., Janus plasmonic-magnetic gold-iron oxide nanoparticles as contrast agents for multimodal imaging. *Nanoscale* **2017,** *9* (27), 9467-9480.

6. Ravel, B.; Newville, M., ATHENA, ARTEMIS, HEPHAESTUS: data analysis for X-ray absorption spectroscopy using IFEFFIT. *Journal of Synchrotron Radiation* **2005,** *12* (4), 537-541.

7. Rehr, J. J.; Albers, R. C., Theoretical approaches to X-ray absorption fine structure. *Reviews of Modern Physics* **2000,** *72* (3), 621.